

Preparation of ZnIn_2S_4 nanosheet-coated CdS nanorod heterostructures for efficient photocatalytic reduction of Cr(VI)

Guping Zhang, Dongyun Chen*, Naijun Li, Qingfeng Xu, Hua Li, Jinghui He, Jianmei Lu*

Collaborative Innovation Center of Suzhou Nano Science and Technology, College of Chemistry Chemical Engineering and Materials Science, Soochow University, 199 Ren'ai Road, Suzhou 215123, PR China



ARTICLE INFO

Keywords:
 $\text{ZnIn}_2\text{S}_4/\text{CdS}$ composite
 Three-dimensional (3D) structure
 Visible light
 Hexavalent chromium (Cr(VI))

ABSTRACT

Nowadays, hexavalent chromium (Cr(VI)) in wastewater seriously threatens ecological systems and human health due to its acute toxicity and potential carcinogenicity. Simultaneously, semiconductor photocatalytic reduction is gaining increasing significant research attention in the treatment of Cr(VI). Hence, three-dimensional (3D) $\text{ZnIn}_2\text{S}_4/\text{CdS}$ composite photocatalysts, assembled by 1D CdS nanorods and 2D ZnIn_2S_4 nanosheets, were prepared *via* a hydrothermal method for reduction of Cr(VI). The composition, microstructure, surface elements and optical properties of the $\text{ZnIn}_2\text{S}_4/\text{CdS}$ composites were thoroughly characterized by X-ray diffraction (XRD), scanning electron microscopy (SEM), X-ray photoelectron spectroscopy (XPS) and UV-vis diffuse reflectance spectroscopy. The as-prepared $\text{ZnIn}_2\text{S}_4/\text{CdS}$ composites showed higher photocatalytic activity for reduction of Cr(VI) compared with pure CdS and ZnIn_2S_4 under visible light irradiation. Meanwhile, the $\text{ZnIn}_2\text{S}_4/\text{CdS}$ composite with a mole ratio of 0.33:1 displayed the best photocatalytic activity, with the efficiency for reduction of Cr(VI) (50 mg/L) reaching 100% within 30 min. The 3D heterostructure not only provided a large surface area, but also effectively separated photogenerated electrons and holes. Importantly, the structure and activity of the catalyst were maintained after three cycles, showing its superior stability. The photocatalytic mechanism of the as-prepared composites was also discussed in detail.

1. Introduction

Rapid urbanization and industrialization have given rise to increasing pollution of water by various heavy metal ions, which has become a serious environmental problem across the globe [1,2]. Among the many heavy metal pollutants, hexavalent chromium (Cr(VI)) seriously threatens ecological systems as well as human health because of its high solubility, acute toxicity and potential carcinogenicity [3]. Therefore, many methods and technologies have been developed for Cr (VI) removal in wastewater in the past decades, including ion exchange [4], membrane separation [5], chemical precipitation and adsorption [6]. However, these traditional methods have several shortcomings, such as high cost and energy consumption, low efficiency and incomplete removal, which hinder their widespread application [7]. In this context, photocatalytic reduction is widely gaining attention as an efficient, green and promising approach, compared with the traditional methods, to treat Cr(VI)-bearing pollutants [8,9].

The advantages of photocatalytic reduction include high efficiency, low cost, lack of secondary pollution and direct use of natural solar energy [10]. In general, when photocatalysts are irradiated by light

with photon energies higher than their band gaps, electrons in the valence bands (VBs) are excited into the conduction bands (CBs) and reduce Cr(VI) to Cr(III) in aquatic environments. However, the photo-generated electrons (e^-) and holes (h^+) of traditional single-component photocatalysts can easily recombine, which suppresses their photocatalytic activity and restricts the extensive application of these devices under sunlight [11,12]. In comparison with single-component photocatalysts, composite photocatalysts can achieve greatly improved photocatalytic activity, mainly because their heterojunctions help to separate photogenerated electrons and holes through interfacial charge transfer [3,13,14]. For example, Tian and co-workers have been prepared $\text{Mn}_3\text{O}_4@\text{ZnO}/\text{Mn}_3\text{O}_4$ heterojunctions for photocatalytic reduction of Cr(VI). This new photocatalyst displayed enhanced photocatalytic activity; The Cr(VI) (200 mL, 10 mg/L) could be reduced completely within 70 min under simulated sunlight irradiation [7]. Sounak's group have been synthesized magnetic and recoverable $\text{TiO}_2/\text{Fe}_3\text{O}_4$ heterostructure successfully, which showed the higher photocatalytic activity than bulk TiO_2 toward Cr(VI) photoreduction in aerobic atmosphere. Because the $\text{TiO}_2/\text{Fe}_3\text{O}_4$ junction could greatly enhanced the charge generation and suppresses the charge

* Corresponding authors.

E-mail addresses: dychen@suda.edu.cn (D. Chen), lujm@suda.edu.cn (J. Lu).

recombination [8]. Therefore, significant research attention is being paid to a range of composite photocatalysts for the photocatalytic reduction of Cr(VI).

Additionally, semiconducting metal sulfides efficiently absorb light in the visible region, making them a promising class of visible-light-driven photocatalysts [15]. Among them, cadmium sulfide (CdS) has drawn intensive attention for two main reasons [16,17]. First, CdS has a narrow band gap of about 2.4 eV, which enables it to absorb and make effective use of light. Second, it can be easily synthesized in the form of various nanostructures, such as nanorods, nanoflowers and nanoparticles. However, the photocatalytic activity of pure CdS is still low because of severe photocorrosion and fast recombination of electron-hole pairs under visible light [18,19]. Extensive previous studies have demonstrated that the formation of heterojunctions with another semiconductor is an effective strategy to overcome these drawbacks [20]. Recently, Yang' group have been synthesized CdS-Sn₂S₃@rGO eutectic cluster heterostructures, which can display increased visible-light-driven photocatalytic activity and strong durability both in photocatalytic hydrogen evolution and Cr(VI) reduction [21].

As an important ternary chalcogenide semiconductor, ZnIn₂S₄, which can be prepared with layered structures, is typically regarded as a good photocatalyst because of its strong visible absorption and excellent chemical stability [22,23]. At an earlier time, Wang and co-workers have been synthesized ZnIn₂S₄ via a facile hydrothermal method for reduction of aqueous Cr(VI). It was found that the as-synthesized ZnIn₂S₄ was much more efficient than In₂S₃, ZnS and P25 TiO₂ in the photocatalytic reduction of aqueous Cr(VI) [24]. Nonetheless, the photocatalytic performance over pure ZnIn₂S₄ is also low because of the short lifetimes of the photogenerated electron-hole pairs [25]. However, it is worth noting that ZnIn₂S₄ and CdS can form a heterojunction with a matched band gap structure, which allows both the effective separation of electrons and holes and their migration between ZnIn₂S₄ and CdS, and accordingly increases the photocatalytic activity of both sulfides [26,27]. Moreover, although ZnIn₂S₄ and its composites have been widely studied for photocatalytic H₂ production in recent years [22,28–30], there are few reports of their use in the reduction of aqueous Cr(VI).

In this study, 3D photocatalysts composed of ZnIn₂S₄ nanosheets and CdS nanorods with different ZnIn₂S₄ mole ratios are prepared by a simple hydrothermal method, as shown in **Scheme 1**. The growth of 2D ZnIn₂S₄ nanosheets on the surface of 1D CdS nanorods to form 3D heterostructures not only increases the surface area, but also effectively promotes electron transfer and separation. The as-prepared 3D ZnIn₂S₄/CdS photocatalysts show considerable photocatalytic activity, with the efficiency for reduction of Cr(VI) (50 mg/L) reaching 100%

within 30 min under visible light irradiation. Finally, a possible mechanism for the improved photocatalytic activity of the 3D ZnIn₂S₄/CdS composites is also proposed in light of the experimental results.

2. Experimental section

2.1. Materials and reagents

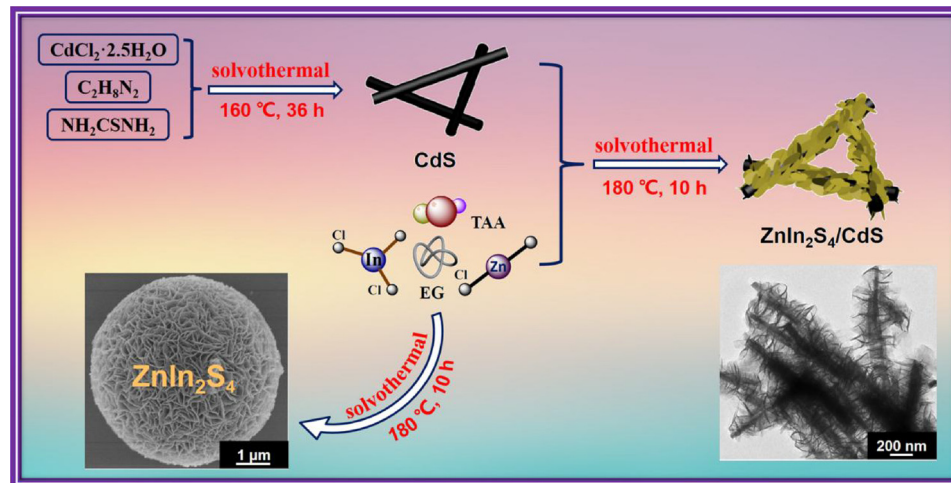
All chemicals and reagents for synthesis and analysis are used as received without further purification. Ethylenediamine (C₂H₈N₂), N, N-dimethylformamide (DMF), glycerol (GL), absolute ethanol (C₂H₅OH) were all agent-grade and purchased from Sinopharm Chemical Reagent Co. Ltd. (China). Cadmium chloride (CdCl₂·2.5H₂O), zinc chloride (ZnCl₂) and Indium chloride tetrahydrate (InCl₃·4H₂O) were all bought from Sinopharm Chemical Reagent Co. Ltd. (China). Thiourea (NH₂CSNH₂) and thioacetamide (TAA) were obtained from Sigma-Aldrich. The water used in all experiments was obtained from a Millipore system (18.2 MΩ cm).

2.2. Preparation of CdS nanorods

The CdS nanorods were synthesized by using a solvothermal method [20]. In a typical experiment, CdCl₂·2.5H₂O (5 mmol) and NH₂CSNH₂ (30 mmol) were added into a 50 mL Teflon-lined stainless steel autoclave containing solution of ethylenediamine (40 mL) and magnetic stirred for half hour. Then, the autoclave was sealed and heated to 160 °C in an electric oven and maintained for 36 h. After that, the products were collected by centrifugation (8000 rpm) and washed several times with deionized water and ethanol. Finally, the bright yellow powder was obtained after drying at 60 °C overnight in a vacuum oven.

2.3. Preparation of ZnIn₂S₄/CdS composites

The ZnIn₂S₄/CdS composites at various mole ratios (0.25:1, 0.33:1, 0.50:1 and 1:1) were prepared by a one-step solvothermal method [28,30]. In detail, ZnCl₂ (0.25–1 mmol), and InCl₃·4H₂O (0.5–2 mmol) and thioacetamide (TAA, 1–4 mmol) were dispersed into the mixture of DMF (15 mL) and GL (5 mL) by ultrasonication for half hour. Next, CdS nanorods (1 mmol) were added into the mixture with the aid of sonication for another half hour at room temperature. Finally, the above mixture was transferred into a 25 mL Teflon-lined stainless steel autoclave, which was heated to 180 °C for 10 h. After cooling to the room temperature, the precipitates were washed several times using water and absolute ethanol and dried at 60 °C overnight in a vacuum oven.



Scheme 1. Schematic illustration of the fabrication of 3D ZnIn₂S₄ nanosheets/CdS nanorods photocatalysts.

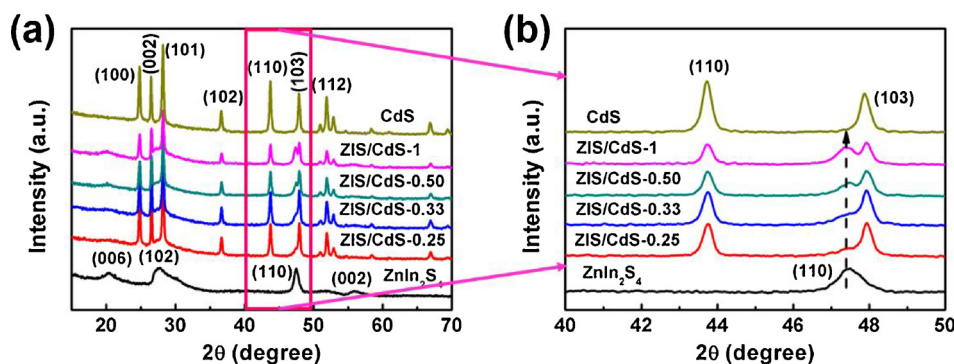


Fig. 1. XRD patterns of the CdS nanorods, ZnIn_2S_4 nanosheets and $\text{ZnIn}_2\text{S}_4/\text{CdS}$ composite photocatalysts with different mole ratios.

For ease of description, as-prepared products with different amounts of ZnIn_2S_4 (0.25–1 mmol) were named as ZIS/CdS-0.25, ZIS/CdS-0.33, ZIS/CdS-0.50 and ZIS/CdS-1, respectively. In addition, pure ZnIn_2S_4 nanosheets were also prepared by a similar method without the introduction of CdS nanorods.

2.4. Characterization

The crystal phase of the samples were analyzed by X-ray diffraction (XRD, X' Pert-Pro MPD). The morphologies and structures of the prepared samples were examined by Scanning electron microscopy (SEM, Hitachi S-4700) and Transmission electron microscopy (TEM, Tecnai G200). The chemical element and the detailed microscopic structure of the samples were investigated by using high-resolution transmission electron microscopy (HRTEM, Tecnai G2 F20 S-TWIN). X-ray photoelectron spectroscopy (XPS) data of the samples were obtained using an X-ray photoelectron spectrometer (ESCALAB MK II) with Al-K α radiation. The specific surface areas were measured with a Micromeritics ASAP 2010 system and analyzed by the Brunauer-Emmett-Teller (BET) method. The diffuse reflectance spectra were measured using a spectrophotometer (UV-vis, DRS Shimadzu UV-3600). The photoluminescence (PL) spectra of the samples were recorded by using a fluorescence spectrophotometer (FLS920) with an excitation wavelength of 385 nm.

2.5. Photoelectrochemical measurements

The photocurrent and electrochemical impedance spectroscopy of the samples were obtained using an electrochemical workstation (CHI 660e, Shanghai, China). A standard three-electrode system was carried out in this photochemical study, the Pt wire was worked as a counter electrode and the Ag/AgCl electrode as a reference electrode. A 0.1 M Na_2SO_4 aqueous solution acted as the electrolyte and a 300 W Xe lamp served as a light source. The working electrodes were prepared as follows: 10 mg of samples were added into 5 mL water and ultrasonication 15 min to form a homogeneous suspension. Then, 2 mL suspension was dropped directly onto the surface of 15 mm \times 45 mm ITO glass. Finally, the ITO glass with samples dried for 0.5 h using an infrared lamp in air.

2.6. Photocatalytic activity measurements

The photocatalytic activities of the as synthesized CdS, ZIS/CdS-0.25-1 and ZnIn_2S_4 were tested for the photocatalytic reduction of Cr (VI) under visible light irradiation using a 300 W Xe lamp with a 400 nm cutoff filter. In each experiment, 50 mg catalyst was added into 50 mL Cr(VI) solution of 50 mg/L which were prepared by dissolving $\text{K}_2\text{Cr}_2\text{O}_7$ into distilled water. Before illumination, the suspension were magnetically stirred in the dark for 1 h at room temperature to obtain absorption-desorption equilibrium. During illumination, approximately 2 mL suspension was sampled from the reactor at given time intervals

with a 0.45 μm membrane filter syringe to remove the photocatalyst. Finally, the Cr(VI) content was measured colorimetrically at $\lambda_{\text{max}} = 540$ nm using the standard diphenylcarbazide (DPC) method [24].

Furthermore, the stability and repeatability of the as synthesized $\text{ZnIn}_2\text{S}_4/\text{CdS}$ composites were investigated by the photocatalytic reduction of Cr(VI). In this study, the $\text{ZnIn}_2\text{S}_4/\text{CdS}$ composite with a mole ratio of 0.33:1 was recycled for three times in the same photocatalytic reactions. After each cycle, the photocatalyst was separated from the suspension by centrifugation (8000 rpm). Then the photocatalyst was soaked in 1 mol/L HNO_3 aqueous in order to remove $\text{Cr}(\text{OH})_3$ deposited on the surface of samples. At last, the photocatalyst was collected by centrifugation (8000 rpm) and washed with deionized water and ethanol, dried in vacuum at 60 °C overnight, and continued for a new cycle.

3. Results and discussion

3.1. XRD analysis

The phase structures of the as-prepared $\text{ZnIn}_2\text{S}_4/\text{CdS}$ samples with different mole ratios of ZnIn_2S_4 were determined by X-ray diffraction (XRD), as shown in Fig. 1a and b. The XRD patterns of pure CdS and ZnIn_2S_4 are also given for comparison. As can be seen from Fig. 1a, all the X-ray peaks for CdS nanorods are assigned to the well-crystallized CdS (JCPDS card 65-3414) [17,20]. Meanwhile, the diffraction peaks at $2\theta = 21.1^\circ$, 27.7° , 47.5° and 56.4° are well indexed to the (006), (102), (110) and (022) crystallographic planes of the hexagonal ZnIn_2S_4 , respectively (JCPDS No.65-2023) [30]. For all $\text{ZnIn}_2\text{S}_4/\text{CdS}$ samples, both CdS and ZnIn_2S_4 phases are observed in these composite materials. Furthermore, it can be found that the diffraction peak intensities of the ZnIn_2S_4 increase with increasing amounts of ZnIn_2S_4 in the composites, along with a decrease of the peak intensities of CdS, as displayed in Fig. 1b. In summary, these results validate the co-existence of ZnIn_2S_4 and CdS in the $\text{ZnIn}_2\text{S}_4/\text{CdS}$ composite materials, and all the as-prepared samples are of high crystallinity with no impurity diffraction peaks.

3.2. SEM and TEM analysis

The morphology and structure of the CdS nanorods, ZnIn_2S_4 nanosheets and $\text{ZnIn}_2\text{S}_4/\text{CdS}$ samples were characterized by scanning electron microscopy (SEM). As illustrated in Figs. S1a and 2 a, the synthesized CdS shows a nanorod-like morphology and a smooth surface, providing a favorable environment for assembling a co-photocatalyst. A typical SEM image of a $\text{ZnIn}_2\text{S}_4/\text{CdS}$ composite ($\text{ZnIn}_2\text{S}_4/\text{CdS}$ mole ratio = 0.33:1) is shown in Fig. 2b. The 2D ZnIn_2S_4 ultrathin nanosheets are uniformly and densely grown on the surface of the 1D CdS nanorods [31]. In addition, the ZnIn_2S_4 nanosheets are interconnected to form a 3D nanosheet network structure (Fig. 2b,c), which

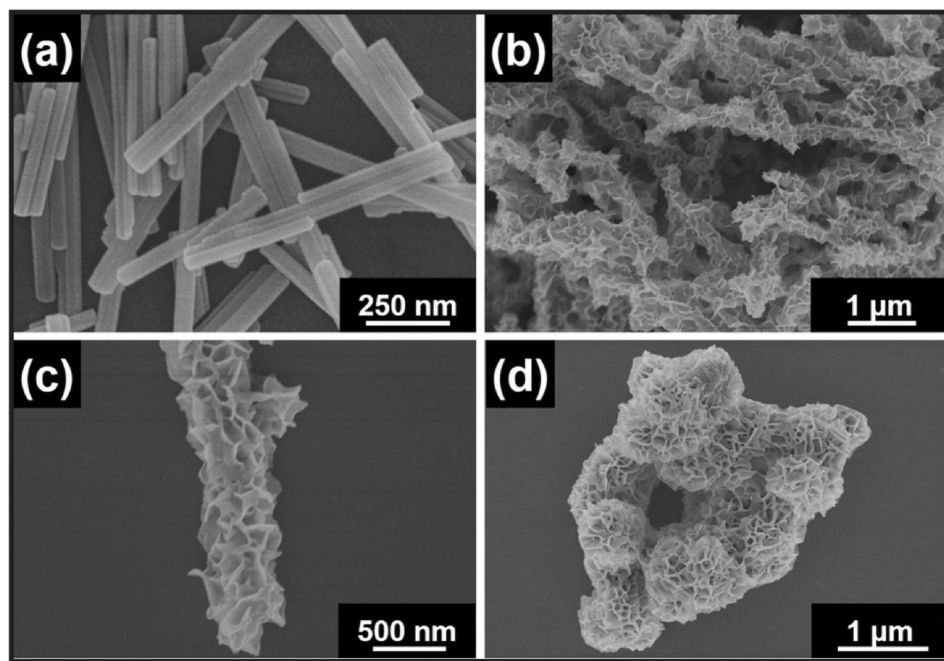


Fig. 2. SEM images of (a) pure CdS nanorods, (b), (c) ZIS/CdS-0.33 composite (ZnIn₂S₄/CdS mole ratio = 0.33:1) and (d) pure ZnIn₂S₄ microspheres assembled from ZnIn₂S₄ nanosheets.

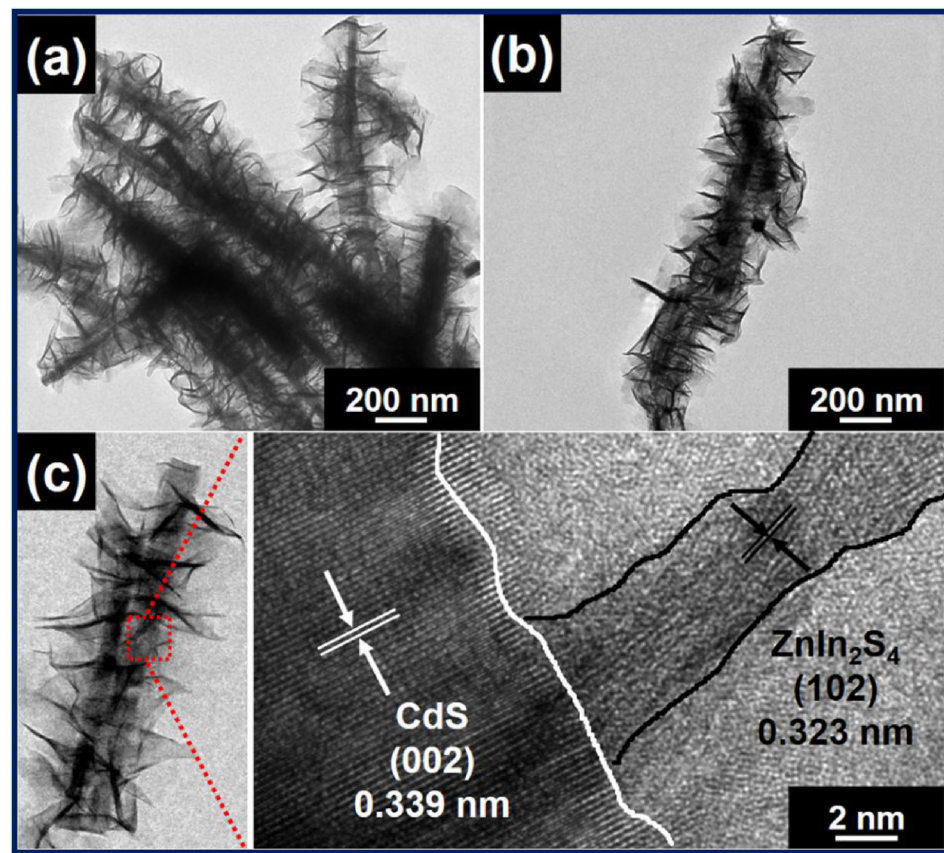


Fig. 3. TEM images of (a), (b) ZIS/CdS-0.33 composite and HRTEM image of (c) ZIS/CdS-0.33 composite (ZnIn₂S₄/CdS mole ratio = 0.33:1).

is beneficial for electron transfer between the two semiconductor materials [28,31]. Meanwhile, ZnIn₂S₄/CdS composite photocatalysts with several different mole ratios (0.25:1, 0.50:1, 1:1) were also obtained, and the corresponding SEM images are presented in Fig. S1b-d. In addition, pure ZnIn₂S₄ nanosheets were prepared by a similar method but in the absence of CdS nanorods, and finally self-assembled into

ZnIn₂S₄ flower-like microspheres (Fig. 2d).

Typical transmission electron microscope (TEM) images of the ZIS/CdS-0.33 composite are shown in Fig. 3a and b. It is clear that the entire surface of the 1D CdS nanorods is fully and densely covered by 2D ZnIn₂S₄ nanosheets. The even distribution of the ZnIn₂S₄ nanosheets on the surface of the CdS nanorods results in the formation of ZnIn₂S₄/CdS

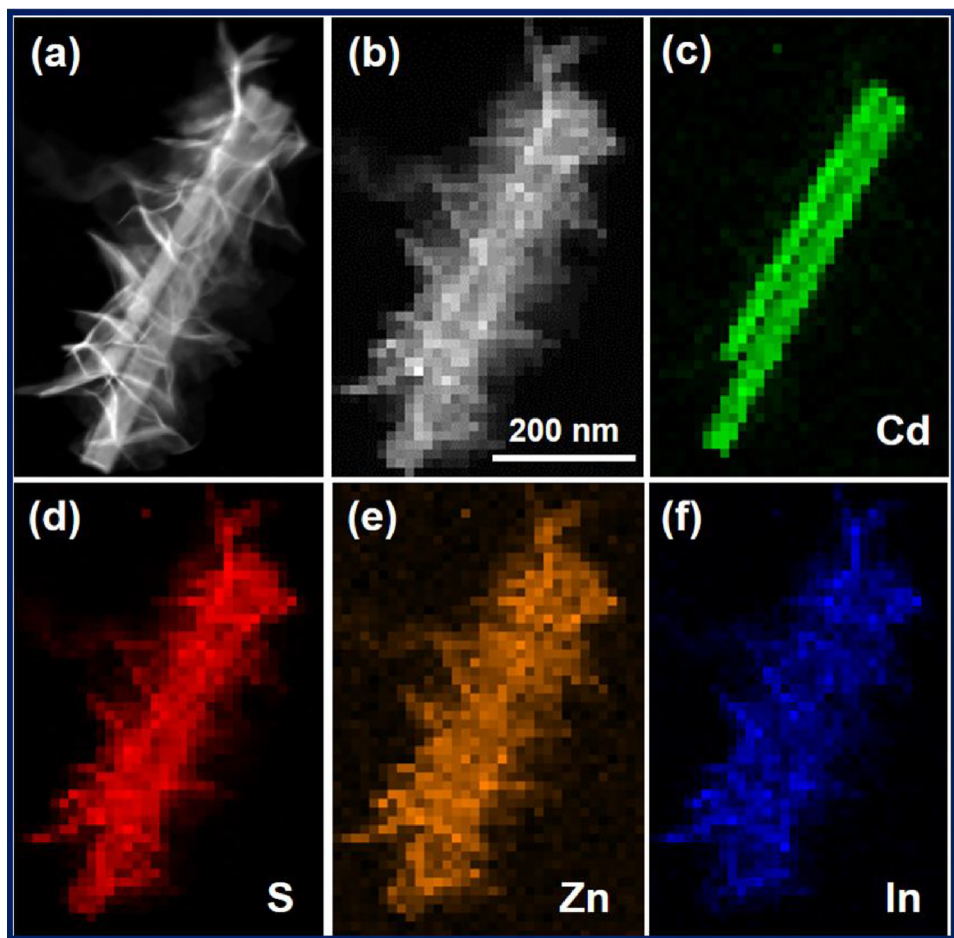


Fig. 4. HAADF-STEM image of (a), (b) and elemental mapping images of (c)–(f) ZIS/CdS-0.33 composite.

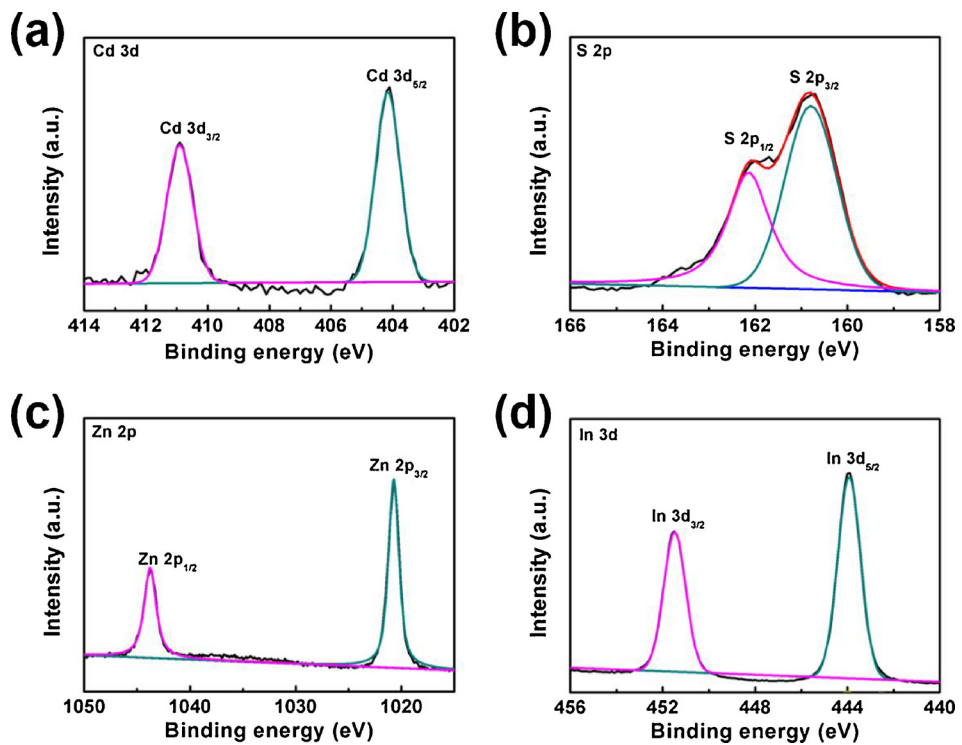


Fig. 5. High-resolution XPS spectra of (a) Cd 3d, (b) S 2p, (c) Zn 2p, (d) In 3d of ZIS/CdS-0.33 composite.

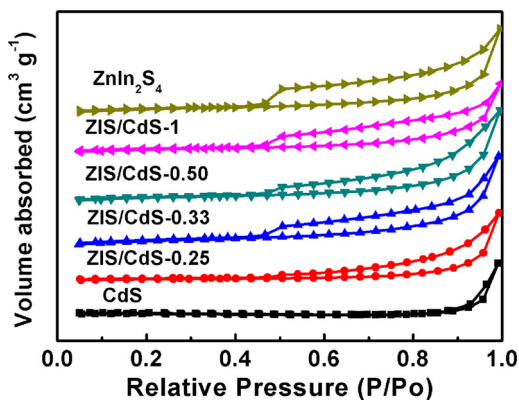


Fig. 6. N_2 adsorption-desorption isotherms of CdS nanorods, ZnIn_2S_4 nanosheets and $\text{ZnIn}_2\text{S}_4/\text{CdS}$ composite photocatalysts with different mole ratios.

Table 1

Surface area (S_{BET}), band gap (E_g) and photocatalytic activities of the as-prepared samples.

| Samples | S_{BET} (m^2/g) | E_g (eV) | DAA (%) | K (min^{-1}) | R^2 |
|---------------------------|--|------------|---------|---------------------------|--------|
| CdS | 7.6736 | 2.38 | 9.38 | 0.0245 | 0.9957 |
| ZIS/CdS-0.25 | 22.7751 | 2.41 | 23.39 | 0.0776 | 0.9806 |
| ZIS/CdS-0.33 | 25.4724 | 2.40 | 24.31 | 0.1790 | 0.9810 |
| ZIS/CdS-0.50 | 28.2440 | 2.42 | 23.01 | 0.1611 | 0.9761 |
| ZIS/CdS-1 | 30.2894 | 2.41 | 22.80 | 0.0930 | 0.9907 |
| ZnIn_2S_4 | 33.4682 | 2.58 | 20.20 | 0.0562 | 0.9916 |

DAA = dark adsorption amount for Cr(VI).

structures with fibrous morphology [28]. The corresponding HRTEM image in Fig. 3c further confirms the intimate contact between CdS nanorods and ZnIn_2S_4 nanosheets. As indicated on Fig. 3c, the lattice spacing is 0.339 nm, which corresponds to the (002) planes of CdS [20]. Lattice fringes with a spacing of 0.323 nm can also be discerned, which represent the (102) crystal plane of ZnIn_2S_4 [22,23,26,30]. Additionally, the TEM images of pure CdS nanorods, and of $\text{ZnIn}_2\text{S}_4/\text{CdS}$ composite photocatalysts with different mole ratios, are shown in Fig. S2a-d.

The structure of the $\text{ZnIn}_2\text{S}_4/\text{CdS}$ composite photocatalyst with a mole ratio of 0.33:1 was further confirmed by elemental mapping analysis (Fig. 4a-f). The elemental mapping indicates the presence of Cd and S (CdS) in the core of the composite. Meanwhile, the elements S, Zn and In (indicating ZnIn_2S_4) are homogeneously distributed throughout the whole composite, and no other elements are present. Therefore, the EDS mapping analysis of 3D $\text{ZnIn}_2\text{S}_4/\text{CdS}$ confirmed the core (CdS nanorods) and shell (ZnIn_2S_4 nanosheets) hierarchical structure [30,31].

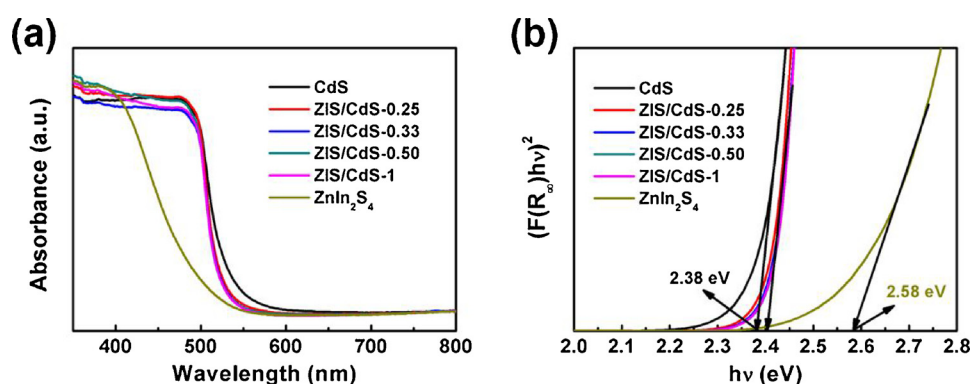


Fig. 7. (a) UV-vis diffuse reflectance absorption spectra (DRS) of the different samples. (b) Plots of $(F(R_\infty)h\nu)^2$ versus $(h\nu)$ for estimating the optical band gaps of the different samples. (For interpretation of the references to colour in this figure legend, the reader is referred to the web version of this article.)

3.3. XPS analysis

To further investigate the surface elemental composition and chemical states of the $\text{ZnIn}_2\text{S}_4/\text{CdS}$ composite photocatalysts, the ZIS/CdS-0.33 sample was analyzed by X-ray photoelectron spectroscopy (XPS). The survey XPS spectra in Fig. S2 show that the composite is mainly composed of Cd, S, Zn and In, which is consistent with the EDS mapping analysis. Meanwhile, the high-resolution XPS spectra of Cd, S, Zn and In elements in the ZIS/CdS-0.33 sample are displayed in Fig. 5. As shown in Fig. 5a, the two strong peaks located at 404.2 and 411.3 eV correspond to the Cd $3d_{5/2}$ and Cd $3d_{3/2}$ states of Cd(II) in CdS, respectively [17,20]. The XPS spectra in Fig. 5b show the binding energy values of S $2p_{3/2}$ and S $2p_{1/2}$ at 160.8 and 162.1 eV, which can be attributed to S^{2-} ions [27]. In addition, the high-resolution Zn 2p spectra (Fig. 5c) display characteristic peaks located at 1020.7 and 1043.8 eV, corresponding to Zn $2p_{3/2}$ and Zn $2p_{1/2}$ binding energies, respectively. Fig. 5d presents the In 3d spectra of the ZIS/CdS-0.33 sample. The two peaks at 444.1 and 451.5 eV are assigned to In $3d_{5/2}$ and In $3d_{3/2}$, respectively [27,30]. These XPS results are in good agreement with previous reports and further indicate the co-existence of CdS and ZnIn_2S_4 in the $\text{ZnIn}_2\text{S}_4/\text{CdS}$ composite photocatalysts.

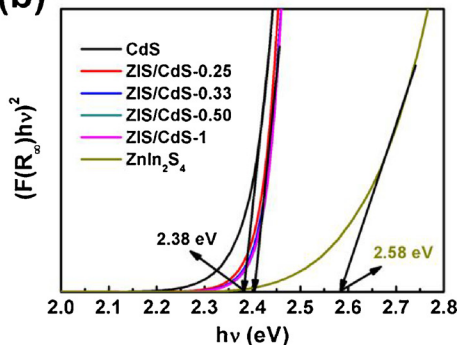
3.4. BET surface area analysis

The surface areas of pure CdS, ZnIn_2S_4 and $\text{ZnIn}_2\text{S}_4/\text{CdS}$ composites were investigated by N_2 adsorption-desorption experiments, and the results are shown in Fig. 6 and Table 1. As can be seen in Fig. 6, all the $\text{ZnIn}_2\text{S}_4/\text{CdS}$ composites displayed type IV isotherms with obvious hysteresis ($P/P_0 = 0.4$ –1.0) between the adsorption and desorption branches, indicating the presence of mesopores [10,15,30]. Moreover, the BET surface areas of the $\text{ZnIn}_2\text{S}_4/\text{CdS}$ composites were much higher than that of pure CdS (Table 1) after the uniform growth of ZnIn_2S_4 nanosheets on the surface of the CdS nanorods. This suggests that a 3D heterostructure with a higher surface area may provide more active sites for adsorption and reduction of Cr(VI), enhancing the photocatalytic activity of the photocatalysts [28,31].

3.5. UV-vis absorption spectra analysis

The optical absorption properties of pure CdS, ZnIn_2S_4 and the $\text{ZnIn}_2\text{S}_4/\text{CdS}$ composite materials with different mole ratios of ZnIn_2S_4 were examined by UV-vis absorption spectroscopy, and the spectra are displayed in Fig. 7a. After the growth of ZnIn_2S_4 nanosheets on the CdS nanorods, the absorption edge of the $\text{ZnIn}_2\text{S}_4/\text{CdS}$ composites showed a slight blue shift in comparison with pure CdS. This may be an effect of the heterostructure formed between CdS and ZnIn_2S_4 [31,32]. However, compared with bare ZnIn_2S_4 , an obvious red shift in the DRS of the $\text{ZnIn}_2\text{S}_4/\text{CdS}$ composites was observed. This red shift might indicate that the composites absorb visible light more strongly in comparison

(b)



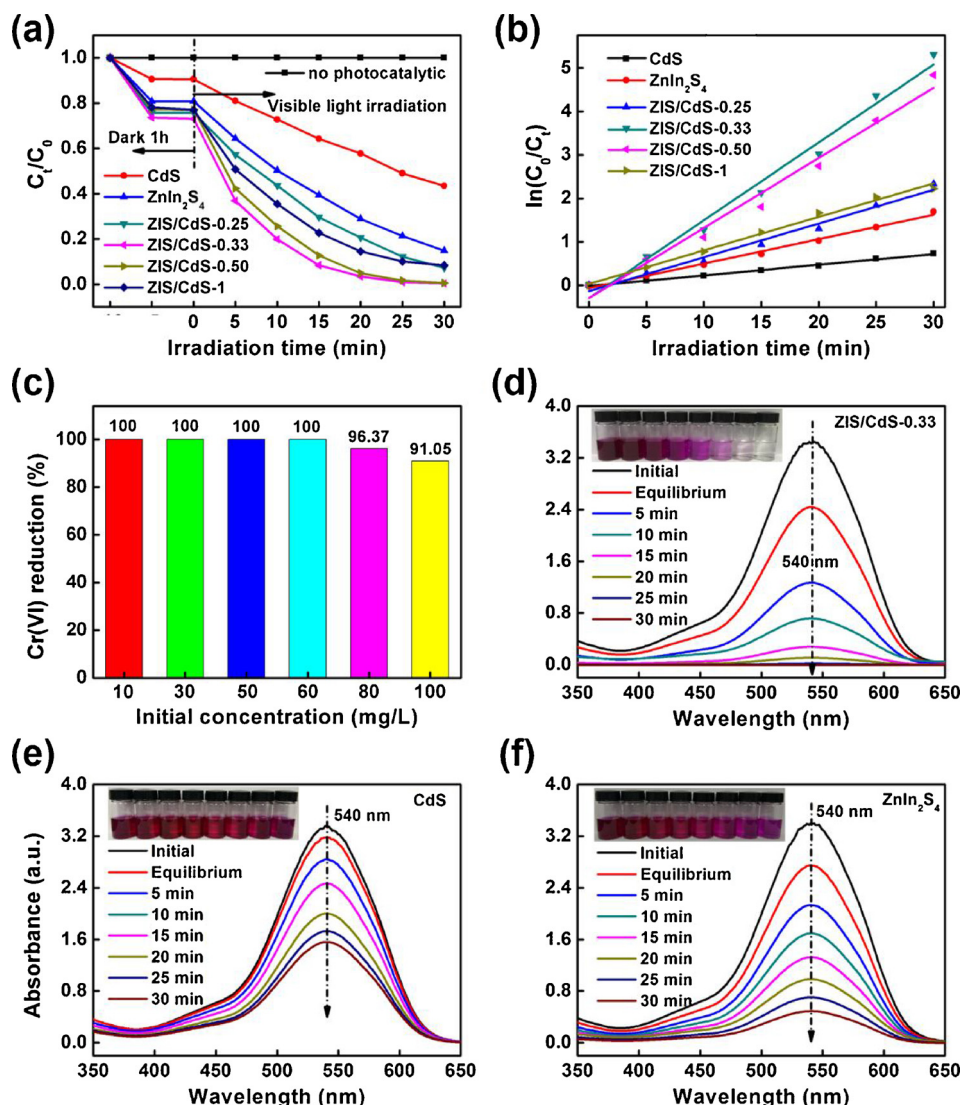


Fig. 8. (a) Photocatalytic activities of CdS, ZIS/CdS-(0.25–1) and ZnIn₂S₄ in the reduction of aqueous Cr(VI) under visible light irradiation. (b) Reaction kinetics for photoreduction of aqueous Cr(VI) with CdS, ZIS/CdS-(0.25–1) and ZnIn₂S₄. (c) Cr(VI) reduction efficiencies of 50 mg of ZIS/CdS-0.33 under visible light for 30 min with different initial Cr(VI) concentrations. (d–f) UV-vis absorption spectra of aqueous Cr(VI) (50 mg/L) treated with ZIS/CdS-0.33, CdS and ZnIn₂S₄ samples.

Table 2

Data comparison of photocatalytic Cr(VI) reduction over different catalysts.

| catalyst | Catalyst (mg) | K ₂ Cr ₂ O ₇ (ppm) | Solution (mL) | K ₂ Cr ₂ O ₇ /catal (mg/mg) | Time (min) | ref |
|---|---------------|---|---------------|--|------------|------|
| SnS ₂ | 300 | 50 | 300 | 0.05 | 120 | [10] |
| SnS ₂ /TiO ₂ | 300 | 50 | 300 | 0.05 | 100 | [12] |
| In-SnS ₂ + HCOOH | 100 | 20 | 250 | 0.05 | 60 | [33] |
| g-C ₃ N ₄ + citric acid | 300 | 50 | 300 | 0.05 | 180 | [34] |
| Agl/BiOI/Bi ₂ O ₃ | 50 | 23.5 | 50 | 0.0235 | 90 | [35] |
| This work | 50 | 50 | 50 | 0.05 | 30 | |

with bare ZnIn₂S₄ [28,30]. According to a previous study, the band gaps (E_g) of the above samples can be obtained from plots of $(F(R_\infty)h\nu)^2$ versus photon energy ($h\nu$) [10,13]. As shown in Fig. 7b, the band gaps of CdS and ZnIn₂S₄ are estimated as 2.38 eV and 2.58 eV, respectively. Meanwhile, the E_g values of ZIS/CdS-(0.25–1) are estimated to be 2.40–2.42 eV (Table 1). Taken together, these results imply that the ZnIn₂S₄/CdS composites can use the full spectrum of visible light to generate photoelectrons and holes because of their suitable band gaps.

3.6. Photocatalytic activity

The photocatalytic activities of the as-prepared samples were evaluated by photocatalytic reduction of aqueous Cr(VI) under visible light. Before irradiation, the suspensions were magnetically stirred in darkness for 60 min to establish the absorption-desorption equilibrium, and the dark adsorption amounts of Cr(VI) on the different samples are shown in Table 1. As illustrated in Fig. 8a, the concentration of Cr(VI) showed almost no change throughout the process in the absence of photocatalysts. This indicated that aqueous Cr(VI) did not spontaneously undergo the photolytic reaction under visible light irradiation

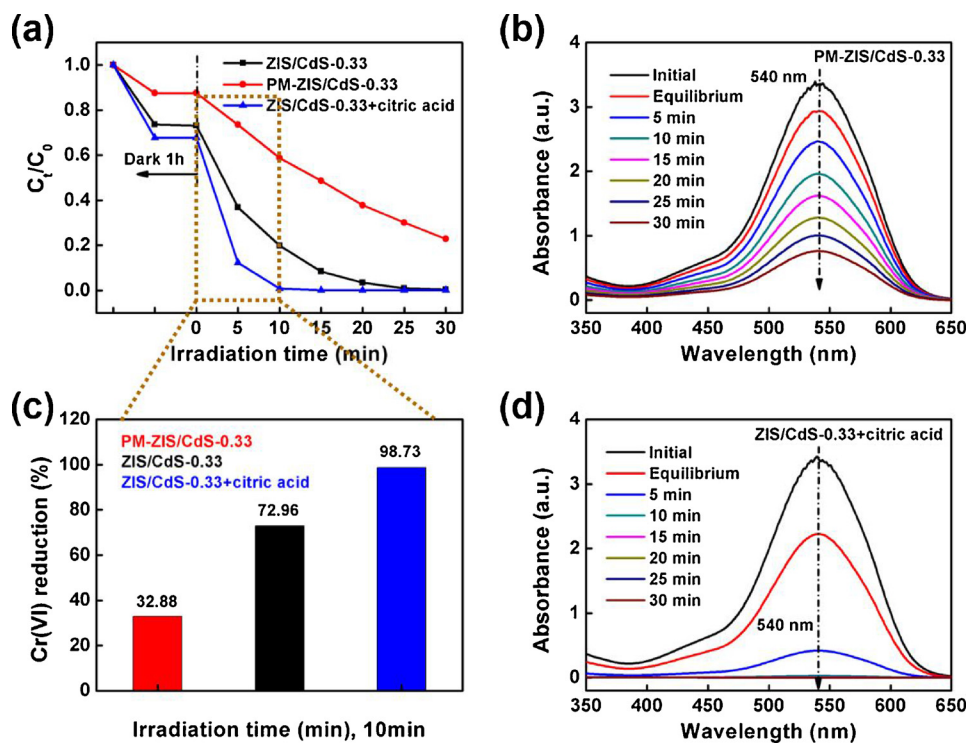


Fig. 9. (a), (c) Comparison of the Cr(VI) reduction efficiencies over ZIS/CdS-0.33, PM-ZIS/CdS-0.33 and ZIS/CdS-0.33 + 0.5 mL citric acid. (b), (d) UV-vis absorption spectra of Cr(VI) (50 mg/L) solution treated with PM-ZIS/CdS-0.33 and ZIS/CdS-0.33 + 0.5 mL citric acid samples.

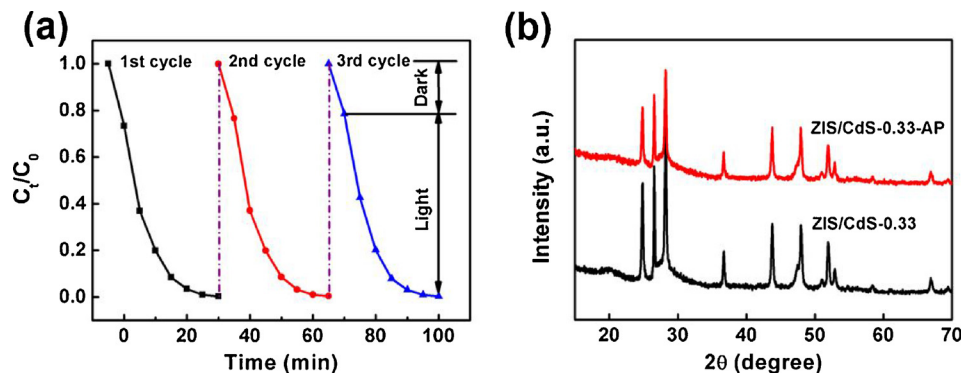


Fig. 10. (a) Cyclic performance of ZIS/CdS-0.33 for the reduction of aqueous Cr(VI) under visible light irradiation. (b) XRD patterns of ZIS/CdS-0.33 and ZIS/CdS-0.33-AP (ZIS/CdS-0.33 recovered after three cycles of photocatalytic use).

and the photocatalysts played an essential role in the reduction of aqueous Cr(VI) [7]. Moreover, all the $\text{ZnIn}_2\text{S}_4/\text{CdS}$ composites exhibited higher photocatalytic activity compared with pure CdS and ZnIn_2S_4 under the same conditions. The greatly enhanced photocatalytic activity of the $\text{ZnIn}_2\text{S}_4/\text{CdS}$ composites can be partly attributed to the strong adsorption of Cr(VI) molecules [31]. Another significant contributing factor is that the ZnIn_2S_4 nanosheets and CdS nanorods formed a heterostructure with matched energy bands, which promoted the transfer and separation of electrons (e^-) and holes (h^+) [27,28,31]. It was also observed that the content of ZnIn_2S_4 affected the Cr(VI) reduction activity, and ZIS/CdS-0.33 displayed the greatest efficiency for photocatalytic reduction of aqueous Cr(VI). As can be seen from Fig. 8d, the absorption peak intensity of Cr(VI) at 540 nm gradually decreased with increasing irradiation time. After irradiation for 30 min, the characteristic absorption peak intensity fell to zero, indicating that the heavy metal pollutant Cr(VI) had been completely reduced. For comparison, the UV-vis absorption spectral changes for aqueous Cr(VI) in the presence of CdS and ZnIn_2S_4 are also shown in Fig. 8e and f, respectively. In addition, the kinetic curves of

photocatalytic reduction of aqueous Cr(VI) with photocatalysts of different compositions are depicted in Fig. 8b. All the kinetic curves were linear and the photoreduction of Cr(VI) followed a pseudo-first-order kinetic model (Eq. (1)) [10]:

$$\ln(C_0/C_t) = kt \quad (1)$$

where t is the irradiation time, k is the kinetic rate constant, C_0 is the initial concentration of Cr(VI) and C_t is the concentration of Cr(VI) at t . Fig. 8b also displays that all of the $\text{ZnIn}_2\text{S}_4/\text{CdS}$ composites had higher Cr(VI) reduction rates than pure CdS and ZnIn_2S_4 . The corresponding kinetic rate constants (k) and R^2 are listed in Table 1. The experimental rate constant k of ZIS/CdS-0.33 was 0.1790 min^{-1} , which was 7.30 times and 3.19 times higher than that of the pure CdS and ZnIn_2S_4 , respectively. Finally, the effect of different initial Cr(VI) concentrations on the photocatalytic reduction performance of 50 mg ZIS/CdS-0.33 was investigated (Fig. 8c). Even when the initial Cr(VI) concentration was as high as 100 mg/L, the ZIS/CdS-0.33 catalyst (50 mg) could still reduce 91.05% of Cr(VI) in 30 min under visible light irradiation (Table 2).

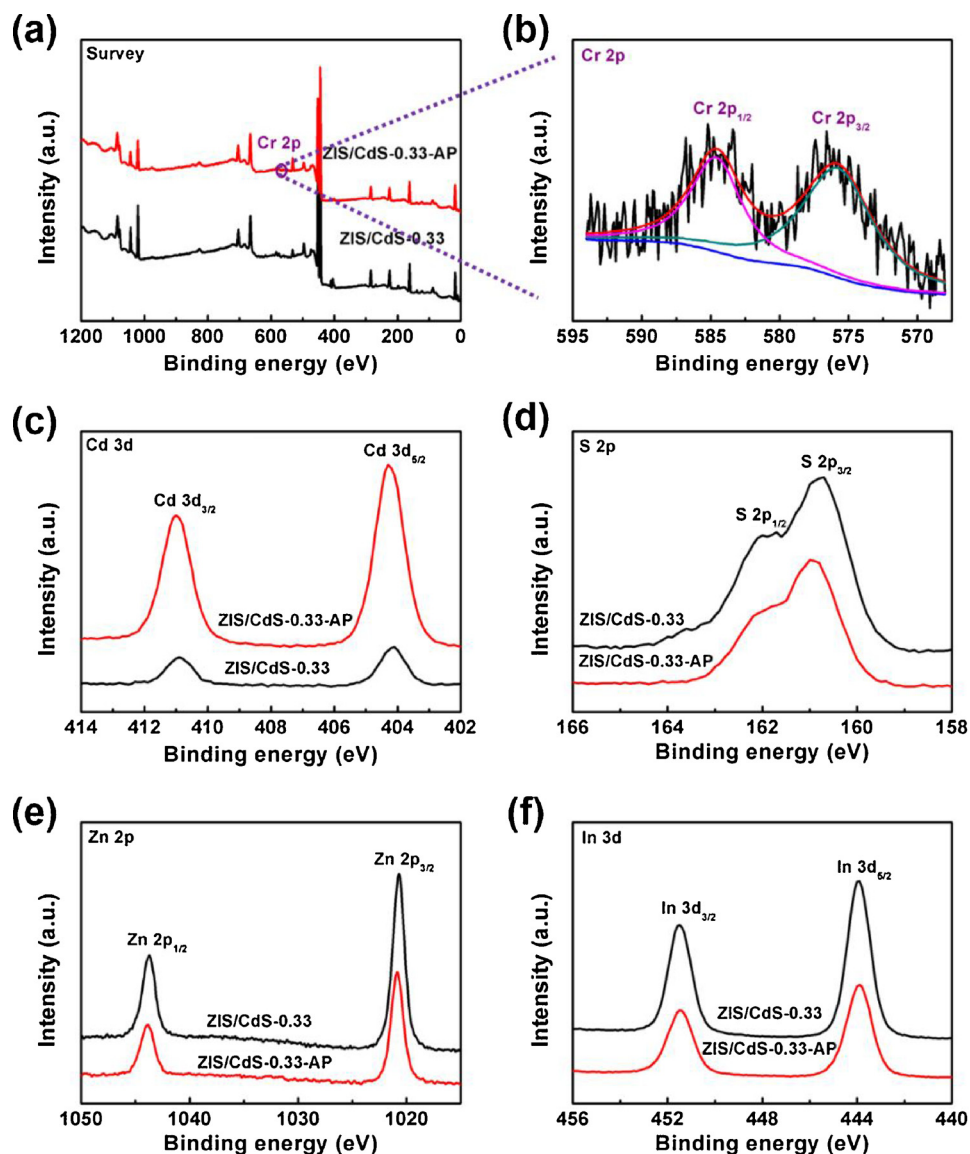


Fig. 11. (a–f) XPS spectra of ZIS/CdS-0.33 and ZIS/CdS-0.33-AP (ZIS/CdS-0.33 recovered after three cycles of photocatalytic use).

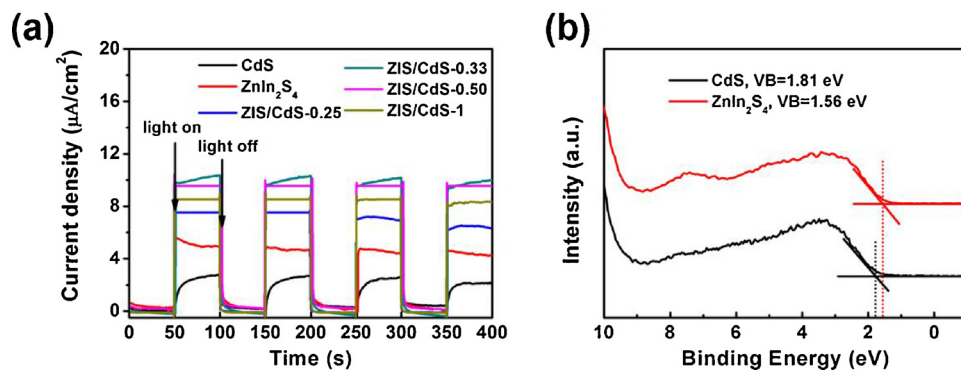
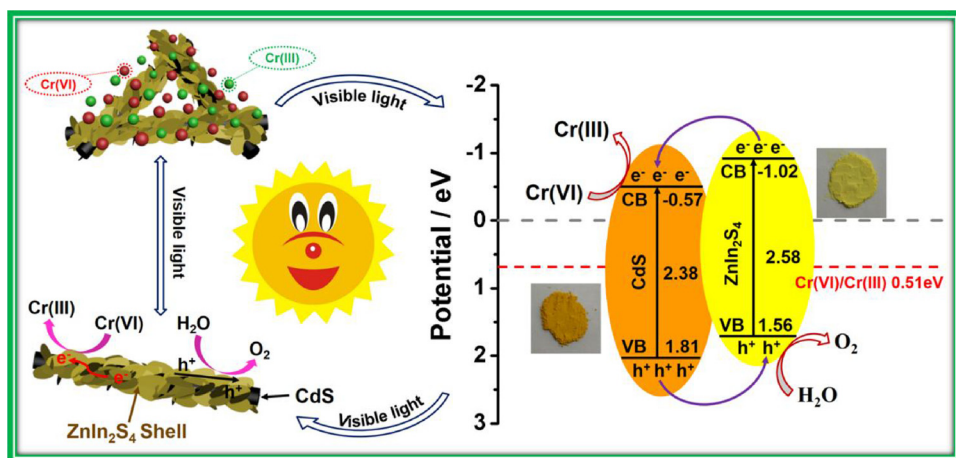


Fig. 12. (a) Transient photocurrent responses of CdS, ZIS/CdS-(0.25–1) and ZnIn₂S₄. (b) Valence band XPS spectra of CdS and ZnIn₂S₄ samples.

Additionally, to confirm the influence of the heterostructure between ZnIn₂S₄ and CdS on the photocatalytic activity, a physical mixture of ZnIn₂S₄ and CdS (0.33:1) was prepared for Cr(VI) photocatalytic reduction under the same conditions. As shown in Fig. 9a, the photocatalytic performance of this physical mixture, denoted PM-ZIS/CdS-0.33, was obviously lower than that of ZIS/CdS-0.33. This indicated

that the heterostructural effect was responsible for promoting electron transfer and separation, thus enhancing the photocatalytic activity [13,23]. At the same time, Fig. 9a also displays the influence of hole scavengers on the visible-light-driven photocatalytic reduction of Cr (VI). The reduction rate of Cr(VI) by ZIS/CdS-0.33 showed an obvious, rapid increase when 0.5 mL citric acid was added to the suspension. The



Scheme 2. Schematic illustration of the reaction mechanism for reduction of Cr(VI) over 3D ZnIn₂S₄/CdS composite under visible light irradiation. (Cr(VI)/Cr(III), 0.51 eV [39]).

reduction rates of Cr(VI) for the ZIS/CdS-0.33 and ZIS/CdS-0.33 + 0.5 mL citric acid systems were 72.96% and 98.73%, respectively, under 10 min light irradiation (Fig. 9c). A plausible mechanism for the improvement of photocatalytic activity is that citric acid was adsorbed on the surface of the photocatalyst, where it easily underwent oxidation by the holes, thus suppressing the recombination of those holes with the electrons [36]. The UV–vis absorption spectral changes of aqueous Cr(VI) for the corresponding samples can be seen in Fig. 9b and d.

Apart from the high Cr(VI) reduction efficiency, the stability of the catalyst is also an important factor in practical applications. Therefore, recycling experiments for the reduction of Cr(VI) under visible light irradiation were conducted with the ZIS/CdS-0.33 sample. As presented in Fig. 10a, the Cr(VI) reduction rate of ZIS/CdS-0.33 showed no obvious decrease after three cycles, indicating that this composite is a stable photocatalyst. In addition, as shown in Fig. 10b, the XRD pattern of the recycled sample, denoted ZIS/CdS-0.33-AP, was consistent with that of the initial sample, with no obvious deviations in the locations of the peaks. Moreover, the elemental composition and chemical states of recycled ZIS/CdS-0.33-AP were also investigated. The XPS spectra in Fig. 11a–f show that ZIS/CdS-0.33-AP contained Cd, S, Zn and In components, as well as Cr contaminants. As shown in Fig. 11c–f, the XPS spectra of ZIS/CdS-0.33-AP were similar to that of the initial sample, with no obvious shifting of the peaks of Cd, S, Zn and In. The binding energy of Cr 2p_{3/2} in ZIS/CdS-0.33-AP was observed at 576.9 eV (Fig. 11b), similar to that of Cr(III) in Cr(OH)₃ [12,30]. Furthermore, both the TEM and SEM images (Fig. S4a–b) also showed that the morphology and structure of ZIS/CdS-0.33 kept well after three cycles of photocatalytic use. Therefore, the above results demonstrate that ZIS/CdS-0.33 has good stability, in addition to its effective ability to reduce Cr(VI) to Cr(III) under visible light irradiation.

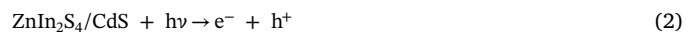
3.7. Possible photocatalytic mechanism

To further investigate the interfacial charge separation efficiency, the photocurrent responses of CdS, ZIS/CdS-(0.25-1) and ZnIn₂S₄ were measured under identical experimental conditions, with the results depicted in Fig. 12a. As can be seen from Fig. 12a, the order of photocurrent response intensity is ZIS/CdS-0.33 > ZIS/CdS-0.50 > ZIS/CdS-1 > ZIS/CdS-0.25 > ZnIn₂S₄ > CdS, which consistent with their results of photocatalytic activity mentioned above. The pure CdS sample shows the lowest photocurrent response, which can be attributed to photocorrosion and fast recombination of photogenerated electron-hole pairs. Meanwhile, the photocurrent response of ZnIn₂S₄ is also relatively weak because of its wide band gap. However, the photocurrent response of ZnIn₂S₄/CdS-(0.25-1) is much higher than that of pure CdS and ZnIn₂S₄, indicating the greater ability of the composite to

effectively separate and transfer charge under visible light irradiation. To further confirm the above results, electrochemical impedance spectroscopy (EIS), a useful measurement to characterize charge carrier transportation, was also tested. As shown in Fig. S5, all ZIS/CdS-(0.25-1) exhibit a smaller diameter of the impedance arc, revealing lower charge transfer resistance in comparison with pure CdS. [7,37,38]. Moreover, the photoluminescence emission spectrum (PL) was performed to observe the process of the separation and recombination of the photogenerated electron–hole pairs. As displayed in Fig. S6, the PL intensity of ZIS/CdS-(0.25-1) is lower than that of pure CdS, which indicates that and recombination of photogenerated electrons and holes, as well as the photocorrosion, can be efficiently inhibited [17,18,20]. Therefore, the results of photocurrent responses and PL demonstrate that the 3D heterostructure between CdS and ZnIn₂S₄ can effectively suppress recombination of photogenerated electrons and holes, and then enhance the corresponding photocatalytic reduction of aqueous Cr(VI).

In addition, to better understand the photocatalytic mechanism of the ZnIn₂S₄/CdS composite, the VBs of CdS and ZnIn₂S₄ were investigated by XPS. The measured XPS VB values of CdS and ZnIn₂S₄ are 1.81 and 1.56 eV, respectively (Fig. 12b). Correspondingly, the CBs of CdS and ZnIn₂S₄ are calculated to be –0.57 and –1.02 eV according to their values of band gap energy (E_g) [7]. These values determined in this study are similar to the previous literatures [14,20,22,30].

Based on the above experimental data and analysis, **Scheme 2** shows a proposed mechanism for the photocatalytic reduction of Cr(VI) by the ZnIn₂S₄/CdS composites. When the ZnIn₂S₄/CdS composites are exposed to visible light irradiation (Eq. 2), both the CdS and ZnIn₂S₄ components are excited and produce photogenerated electrons (e[–]) and holes (h⁺). At the same time, the e[–] from ZnIn₂S₄ can rapidly transfer to the CB of CdS while the h⁺ from CdS can migrate to the VB of ZnIn₂S₄, because the VB and CB potentials of ZnIn₂S₄ are both more negative than those of CdS [26,27]. Therefore, the photogenerated electrons and holes are separated efficiently and their recombination is retarded in the photocatalytic system of ZnIn₂S₄/CdS, leading to greater photocatalytic activity than the pure CdS and ZnIn₂S₄. Finally, Cr₂O₇^{2–} is reduced to Cr(III) by the photogenerated electrons and O₂ is produced by oxidation of H₂O, as displayed in Eqs. (3) and (4).



4. Conclusions

In summary, a series of 3D $\text{ZnIn}_2\text{S}_4/\text{CdS}$ photocatalysts with different ZnIn_2S_4 content were successfully prepared via a hydrothermal method. All the as-prepared $\text{ZnIn}_2\text{S}_4/\text{CdS}$ composites exhibited higher photocatalytic activity compared with pure ZnIn_2S_4 and CdS under visible light irradiation. Specifically, ZIS/CdS-0.33 displayed the greatest photocatalytic activity for reduction of aqueous Cr(VI). The 3D heterostructure effectively promoted charge transfer and suppressed recombination of photogenerated electrons and holes, leading to the enhanced photocatalytic reduction of aqueous Cr(VI). In addition, the $\text{ZnIn}_2\text{S}_4/\text{CdS}$ composites also showed good stability and recycling performance. This study demonstrates that 3D $\text{ZnIn}_2\text{S}_4/\text{CdS}$ composites assembled from 1D and 2D nanostructures are a promising alternative for the reduction of Cr(VI) in wastewater in the future.

Acknowledgements

We gratefully acknowledge the financial support provided by the National Key R&D Program of China (2017YFC0210901, 2017YFC0210906), National Natural Science Foundation of China (51573122, 21722607, 21776190), Natural Science Foundation of the Jiangsu Higher Education Institutions of China (17KJA430014, 17KJA150009), the Science and Technology Program for Social Development of Jiangsu (BE2015637) and the project supported by the Priority Academic Program Development of Jiangsu Higher Education Institutions (PAPD).

Appendix A. Supplementary data

Supplementary material related to this article can be found, in the online version, at doi:<https://doi.org/10.1016/j.apcatb.2018.03.017>.

References

- Y.Z. Yan, Q.D. An, Z.Y. Xiao, S.R. Zhai, B. Zhai, Z. Shi, Interior multi-cavity/surface engineering of alginate hydrogels with polyethylenimine for highly efficient chromium removal in batch and continuous aqueous systems, *J. Mater. Chem. A* 5 (2017) 17073–17087.
- C.C. Wang, X.D. Du, J. Li, X.X. Guo, P. Wang, J. Zhang, Photocatalytic Cr(VI) reduction in metal-organic frameworks: a mini-review, *Appl. Catal. B: Environ.* 193 (2016) 198–216.
- Y.C. Zhang, L. Yao, G. Zhang, D.D. Dionysiou, J. Li, X. Du, One-step hydrothermal synthesis of high-performance visible-light-driven $\text{SnS}_2/\text{SnO}_2$ nanoheterojunction photocatalyst for the reduction of aqueous Cr(VI), *Appl. Catal. B: Environ.* 144 (2014) 730–738.
- Y. Xing, A. Xueming Chen, D. Wang, Electrically regenerated ion exchange for removal and recovery of Cr(VI) from wastewater, *Environ. Sci. Technol.* 41 (2007) 1439–1443.
- U. Divrikli, A.A. Kartal, M. Soylak, L. Elci, Preconcentration of Pb(II), Cr(III), Cu(II), Ni(II) and Cd(II) ions in environmental samples by membrane filtration prior to their flame atomic absorption spectrometric determinations, *J. Hazard. Mater.* 145 (2007) 459–464.
- B. Xie, C. Shan, Z. Xu, X. Li, X. Zhang, J. Chen, B. Pan, One-step removal of Cr(VI) at alkaline pH by UV/sulfite process: reduction to Cr(III) and *in situ* Cr(III) precipitation, *Chem. Eng. J.* 308 (2016) 791–797.
- N. Li, Y. Tian, J. Zhao, J. Zhang, J. Zhang, W. Zuo, Y. Ding, Efficient removal of chromium from water by $\text{Mn}_3\text{O}_4@\text{ZnO}/\text{Mn}_3\text{O}_4$ composite under simulated sunlight irradiation: synergy of photocatalytic reduction and adsorption, *Appl. Catal. B: Environ.* 214 (2017) 126–136.
- S. Challagulla, R. Nagarjuna, R. Ganesan, S. Roy, Acrylic-based polymerizable sol-gel synthesis of magnetically recoverable TiO_2 supported Fe_3O_4 for Cr(VI) photoreduction in aerobic atmosphere, *ACS Sustain. Chem. Eng.* 4 (2016) 169–175.
- D.K. Padhi, T.K. Panigrahi, K.M. Parida, S.K. Singh, P.M. Mishra, Green synthesis of $\text{Fe}_3\text{O}_4/\text{RGO}$ nanocomposite with enhanced photocatalytic performance for Cr(VI) reduction, phenol degradation and antibacterial activity, *ACS Sustain. Chem. Eng.* 5 (2017) 10551–10562.
- Y.C. Zhang, J. Li, M. Zhang, D.D. Dionysiou, Size-tunable hydrothermal synthesis of SnS_2 nanocrystals with high performance in visible light-driven photocatalytic reduction of aqueous Cr(VI), *Environ. Sci. Technol.* 45 (2011) 9324–9331.
- X. An, J.C. Yu, F. Wang, C. Li, Y. Li, One-pot synthesis of In_2S_3 nanosheets/graphene composites with enhanced visible-light photocatalytic activity, *Appl. Catal. B: Environ.* 129 (2013) 80–88.
- Y.C. Zhang, J. Li, H.Y. Xu, One-step *in situ* solvothermal synthesis of $\text{SnS}_2/\text{TiO}_2$ nanocomposites with high performance in visible light-driven photocatalytic reduction of aqueous Cr(VI), *Appl. Catal. B: Environ.* 123–124 (2012) 18–26.
- Y.C. Zhang, Z.N. Du, K.W. Li, M. Zhang, D.D. Dionysiou, High-performance visible-light-driven $\text{SnS}_2/\text{SnO}_2$ nanocomposite photocatalyst prepared via *in situ* hydrothermal oxidation of SnS_2 nanoparticles, *ACS Appl. Mater. Interfaces* 3 (2011) 1528–1537.
- H. Liu, Z. Jin, Z. Xu, Z. Zhang, D. Ao, Fabrication of $\text{ZnIn}_2\text{S}_4-g-\text{C}_3\text{N}_4$ sheet-on-sheet nanocomposites for efficient visible-light photocatalytic H_2 -evolution and degradation of organic pollutants, *RSC Adv.* 5 (2015) 97951–97961.
- C. Mondal, M. Ganguly, J. Pal, A. Roy, J. Jana, T. Pal, Morphology controlled synthesis of SnS_2 nanomaterial for promoting photocatalytic reduction of aqueous Cr(VI) under visible light, *Langmuir* 30 (2014) 4157–4164.
- J. He, L. Chen, F. Wang, Y. Liu, P. Chen, C.T. Au, S.F. Yin, CdS nanowires decorated with ultrathin MoS_2 nanosheets as an efficient photocatalyst for hydrogen evolution, *ChemSusChem* 9 (2016) 624–630.
- X.L. Yin, L.L. Li, W.J. Jiang, Z. Yun, Z. Xiang, L.J. Wan, J.S. Hu, MoS_2/CdS nanosheets-on-nanorod heterostructure for highly efficient photocatalytic H_2 generation under visible light irradiation, *ACS Appl. Mater. Interfaces* 8 (2016) 15258–15266.
- M.Q. Yang, C. Han, Y.J. Xu, Insight into the effect of highly dispersed MoS_2 versus layer-structured MoS_2 on the photocorrosion and photoactivity of CdS in Graphene– CdS – MoS_2 composites, *J. Phys. Chem. C* 119 (2015) 27234–27246.
- Q. Xiang, F. Cheng, D. Lang, Hierarchical layered WS_2 /graphene-modified CdS nanorods for efficient photocatalytic hydrogen evolution, *ChemSusChem* 9 (2016) 996–1002.
- P. Wang, T. Wu, C. Wang, J. Hou, J. Qian, Y. Ao, Combining heterojunction engineering with surface cocatalyst modification to synergistically enhance the photocatalytic hydrogen evolution performance of cadmium sulfide nanorods, *ACS Sustain. Chem. Eng.* 5 (2017) 7670–7677.
- C. Xue, X. Yan, H. An, H. Li, J. Wei, G. Yang, Bonding CdS – SnS_2 eutectic clusters on graphene nanosheets with unusually photoreaction-driven structural reconfiguration effect for excellent H_2 evolution and Cr(VI) reduction, *Appl. Catal. B: Environ.* 222 (2018) 157–166.
- Z. Zhang, K. Liu, Z. Feng, Y. Bao, B. Dong, Hierarchical sheet-on-sheet $\text{ZnIn}_2\text{S}_4/g-\text{C}_3\text{N}_4$ heterostructure with highly efficient photocatalytic H_2 production based on photoinduced interfacial charge transfer, *Sci. Rep.-UK* 6 (2016) 19221.
- Y. Chen, G. Tian, Z. Ren, K. Pan, Y. Shi, J. Wang, H. Fu, Hierarchical core-shell carbon nanofiber@ ZnIn_2S_3 composites for enhanced hydrogen evolution performance, *ACS Appl. Mater. Interfaces* 6 (2014) 13841–13849.
- T.X. Wang, S.H. Xu, F.X. Yang, ZnIn_2S_3 nanopowder as an efficient visible light-driven photocatalyst in the reduction of aqueous Cr(VI), *Mater. Lett.* 83 (2012) 46–48.
- W. Chen, T.Y. Liu, T. Huang, X.H. Liu, X.J. Yang, Novel mesoporous P-doped graphitic carbon nitride nanosheets coupled with ZnIn_2S_4 nanosheets as efficient visible light driven heterostructures with remarkably enhanced photo-reduction activity, *Nanoscale* 8 (2016) 3711–3719.
- B. Xu, P. He, H. Liu, P. Wang, Z. Gang, W. Xun, A 1D/2D helical $\text{CdS}/\text{ZnIn}_2\text{S}_4$ nano-heterostructure, *Angew. Chem. Int. Ed.* 53 (2014) 2339–2343.
- Q. Tian, W. Wu, J. Liu, Z. Wu, W. Yao, J. Ding, C. Jiang, Dimensional heterostructure of 1D CdS /2D ZnIn_2S_4 composites with 2D graphene: designed synthesis and superior photocatalytic performance, *Dalton Trans.* 46 (2017) 2770–2777.
- G. Yang, D. Chen, H. Ding, J. Feng, J.Z. Zhang, Y. Zhu, S. Hamid, D.W. Bahnemann, Well-designed 3D ZnIn_2S_4 nanosheets/ TiO_2 nanobelts as direct Z-scheme photocatalysts for CO_2 photoreduction into renewable hydrocarbon fuel with high efficiency, *Appl. Catal. B: Environ.* 219 (2017) 611–618.
- Y. Chen, G. Tian, W. Zhou, Y. Xiao, J. Wang, X. Zhang, H. Fu, Enhanced photo-generated carrier separation in CdS quantum dot sensitized $\text{ZnFe}_2\text{O}_4/\text{ZnIn}_2\text{S}_4$ nanosheet stereoscopic films for exceptional visible light photocatalytic H_2 evolution performance, *Nanoscale* 9 (2017) 5912–5921.
- H. Liu, J. Zhang, D. Ao, Construction of heterostructured $\text{ZnIn}_2\text{S}_4@\text{NH}_2\text{-MIL}-125(\text{Ti})$ nanocomposites for visible-light-driven H_2 production, *Appl. Catal. B: Environ.* 221 (2018) 433–442.
- W. Zhou, Z. Yin, Y. Du, X. Huang, Z. Zeng, Z. Fan, H. Liu, J. Wang, H. Zhang, Synthesis of few-layer MoS_2 nanosheet-coated TiO_2 nanobelt heterostructures for enhanced photocatalytic activities, *Small* 9 (2013) 140–147.
- D.C. Jiang, Z. Sun, H. Jia, D. Lu, P. Du, A cocatalyst-free CdS nanorod/ ZnS nanoparticle composite for high-performance visible-light-driven hydrogen production from water, *J. Mater. Chem. A* 4 (2015) 675–683.
- S. Park, R. Selvaraj, M.A. Meetani, Y. Kim, Enhancement of visible-light-driven photocatalytic reduction of aqueous Cr(VI) with flower-like In^{3+} -doped SnS_2 , *J. Ind. Eng. Chem.* 45 (2017) 206–214.
- Y. Zhang, Q. Zhang, Q. Shi, Z. Cai, Z. Yang, Acid-treated $g-\text{C}_3\text{N}_4$ with improved photocatalytic performance in the reduction of aqueous Cr(VI) under visible-light, *Sep. Purif. Technol.* 142 (2015) 251–257.
- Q. Wang, X. Shi, E. Liu, J.C. Crittenden, X. Ma, Y. Zhang, Y. Cong, Facile synthesis of $\text{AgI}/\text{BiO}_1\text{-Bi}_2\text{O}_3$ multi-heterojunctions with high visible light activity for Cr(VI) reduction, *J. Hazard. Mater.* 317 (2016) 8–16.
- D. Xiao, K. Dai, Y. Qu, Y. Yin, H. Chen, Hydrothermal synthesis of $\alpha\text{-Fe}_2\text{O}_3/g-\text{C}_3\text{N}_4$ composite and its efficient photocatalytic reduction of Cr(VI) under visible light, *Appl. Surf. Sci.* 358 (2015) 181–187.
- P. Tan, X. Chen, L. Wu, Y.Y. Shang, W. Liu, J. Pan, X. Xiong, Hierarchical flower-like SnSe_2 supported Ag_3PO_4 nanoparticles: towards visible light driven photocatalyst with enhanced performance, *Appl. Catal. B: Environ.* 202 (2017) 326–334.
- P. Xia, B. Zhu, B. Cheng, J. Yu, J. Xu, 2D/2D $g-\text{C}_3\text{N}_4/\text{MnO}_2$ nanocomposite as a direct Z-scheme photocatalyst for enhanced photocatalytic activity, *ACS Sustain. Chem. Eng.* 6 (2018) 965–973.
- R. Liang, L. Shen, F. Jing, W. Wu, Q. Na, L. Rui, W. Ling, NH_2 -mediated indium metal-organic framework as a novel visible-light-driven photocatalyst for reduction of the aqueous Cr(VI), *Appl. Catal. B: Environ.* 162 (2015) 245–251.